ELSEVIER

Metamorphic controls on seismic velocity of subducted oceanic crust at 100–250 km depth

J.A.D. Connolly [a],[*], D.M. Kerrick [b]

[a] *Earth Sciences Department, Swiss Federal Institute of Technology, 8092 Zurich, Switzerland*
[b] *Geosciences Department, Pennsylvania State University, University Park, PA 16802, USA*

Abstract

Most circum-Pacific subduction zones at 100–250 km depth contain layers in which seismic velocities are ca. 5% slower than in the adjacent mantle. We compute seismic velocities from thermodynamic data for equilibrium metabasalt mineralogies, determined by free energy minimization, at subduction zone conditions. Lawsonite stability has a profound effect on seismic velocities of subducted oceanic metabasalts. Velocity reductions of 3–7% are estimated for lawsonite–eclogites derived by metamorphism of hydrothermally altered oceanic basalt subducted along relatively cool geotherms, whereas a 2–4% velocity increase is characteristic of anhydrous eclogites within the coesite stability field. The restricted depth extent of low-velocity layers is explicable through the influence of the coesite–stishovite transition, which reduces lawsonite stability at high pressure. This transition also increases the positive velocity anomaly in anhydrous eclogites to 4–6%, an effect that may account for deep high-velocity layers. The quality of the match between the properties of lawsonite–eclogite and low-velocity layers supports the contention that significant quantities of volatiles are retained within the oceanic crust beyond sub-arc depths. Because the velocity anomalies are explicable in terms of equilibrium phase relations, we find no reason to invoke metastability of metamorphic reactions to explain the low-velocity layers.
© 2002 Elsevier Science B.V. All rights reserved.

Keywords: seismic velocity; low-velocity layers; subduction; devolatilization; metamorphism

1. Introduction

With some exceptions [1,2], seismic waves that travel along the tops of most circum-Pacific subducted slabs at depths of 100–250 km are 3–7% slower than the surrounding mantle [3–8]. To explain these observations geophysical models require homogeneous layers, characterized by unusually low seismic velocities, that extend over the entire depth range of observation [2,9]. Thicknesses estimated for the layers are comparable to, or less than, those of oceanic crust ($\sim$7 km). These estimates, in tandem with a variety of other constraints, have led to the inference that the low-velocity layers correspond to a section of the subducted oceanic crust [2,6–8]. The low seismic wave velocities are attributed to mineralogy, but the specific mineralogy of the low-velocity layers is

---

* Corresponding author. Tel.: +41-1-632-7804;
Fax: +41-1-632-1088.
  E-mail address: james.connolly@erdw.ethz.ch
(J.A.D. Connolly).

controversial. Subducted oceanic crust has traditionally been thought to undergo an equilibrium transition from seismically slow anhydrous gabbroic mineralogies to fast eclogitic mineralogies at depths of 20–50 km. Because this transition is kinetically hindered, the persistence of metastable gabbros was hypothesized to explain low-velocity layers at depths of 60 km [10]. With the discovery of deeper low-velocity layers, this hypothesis has been invoked to explain seismic anomalies at depths > 100 km [4,11]. However, the petrological arguments for metastability are questionable at such depths [6–8], and almost certainly unsustainable at 250 km. Additionally, detailed observations indicate that seismic velocities in metastable gabbroic mineralogies are too slow for these rocks to be the origin of low-velocity layers [8]. Most recently it has therefore been argued that metastable hydrous mineralogies are the most plausible cause for low seismic velocities in subducted slabs at 100–250 km depth [7,8]. This thesis is problematic because if anhydrous gabbros do not persist metastably within the oceanic crust, then it is doubtful that dehydration reactions, which are usually kinetically faster than anhydrous phase transformations, can be suppressed so as to preserve metastable hydrous minerals [12,13]. We show that the predicted stability and seismic properties of lawsonite–eclogites, which form by the progressive metamorphism of metabasalt, may resolve this dilemma.

2. Model formulation and methods

The subducted oceanic crust consists of a relatively thin (< 800 m) heterogeneous layer of marine sediments, an upper 2–3 km thick sequence of layered hydrothermally altered basalts (metabasalts), and a less altered, but more heterogeneous, lower section comprised largely of gabbroic rocks with an average composition similar to the basaltic section [14]. Because seismic velocities for the equilibrium mineralogies of anhydrous metabasic rocks are 2–4% faster those of the ambient mantle at the depths of interest [2], we focus on the upper basaltic section, which should be characterized by greater abundances of seismically slow hydrous

minerals. The stratification and chemical homogeneity of the metabasalts provide additional motivation for this choice, because these features are essential for efficient channeling of seismic energy [2,8]. We neglect the metasediments because their thickness and heterogeneity are inconsistent with geophysical models for low-velocity layers [2,8]. At the depths of interest, the equilibrium mineralogy of the metasediments is similar to that of metabasalt, but metasediments contain greater amounts of hydrous minerals [15–18]. Thus we anticipate that the effect of metasediments, if any, is to enhance the strength of any low-velocity anomaly predicted solely from metabasalt.

It is commonly assumed that the composition of the subducted igneous crust is that of normal mid-ocean ridge basalts (MORB) modified by the addition of water through hydrothermal alteration. However, to a depth of at least 1 km the hydrothermal effects are more complex and involve the introduction of water, CO_2, and modification of the non-volatile composition [19,20]. The correlation of the basaltic section, or indeed the entire crust, with a low-velocity layer would imply that the seismic properties of individual lithologies must be averaged in some manner. Such correlations contrast with the results of detailed seismic dispersion studies that suggest low-velocity layers represent samples of the crust that may be as thin as 2 km [5,8,21]. To constrain seismic velocities in either scenario, we consider the end-member cases of hydrated MORB and metasomatically altered MORB, designated hereafter as 'unaltered' and 'altered' basalt (Table 1). The unaltered composition is that of synthetic high-magnesium MORB that was studied experimentally at the conditions of interest [15,16]. This composition was chosen in preference to a natural composition to verify the accuracy of our computed phase relations. For our altered basalt model we use an averaged bulk composition for the upper 500 m of the igneous crust [19].

Metamorphic devolatilization may be influenced by fluids derived from adjacent rocks and by the rate of fluid expulsion. Evaluation of such effects requires knowledge of the nature of metamorphic fluid flow and lithologic structure. To avoid the loss of generality inherent in specifying

Table 1
List of symbols

Symbol	Meaning
G	molar Gibbs free energy
K_S	adiabatic bulk modulus, Eq. 4
N	molar formula weight
P	pressure
T	temperature
v_S	shear wave (S-wave) velocity, Eq. 1
v_P	compressional (P-wave) wave velocity, Eq. 2
v_S^0, v_P^0	ambient mantle P- and S-wave velocities, Eqs. 6, 7
μ	shear modulus, Eq. 5
ρ	density, Eq. 3

unknown hydrologic properties and lithologic details, we consider three simple models for metabasalt devolatilization to illustrate the extremes likely to be realized in subduction zones. For the unaltered metabasalt, we assume water-saturated conditions, an assumption that maximizes the abundance of hydrous minerals as a function of pressure (P) and temperature (T, see Table 1 for notation). Phase relations computed on this basis are those expected if the fluid chemistry is dominated by water-rich fluids derived from lower crustal rocks that contain little CO_2 [22]. Alternatively, such a model is appropriate in the limits of both a closed system or an open system, in which fluid is expelled as rapidly as it is produced (i.e., Rayliegh fractionation) with the proviso that the initial water content is adequate to generate a

fluid phase. For the altered basalt we employ two closed-system models. The first model, in which we use the bulk composition as stated in Table 2, simulates a scenario in which externally derived fluids do not affect the devolatilization process. Because hydrated minerals generally decompose at a lower temperature than carbonates [17,18], hydrated mineral stabilities in a mixed-volatile closed system are almost identical to those in a system that devolatilizes by Rayliegh fractionation. In contrast, devolatilization by Rayliegh fractionation preserves carbonate minerals to significantly higher temperatures than in a closed system. Despite this effect, we prefer the closed system model because in such a model the devolatilization process is not path-dependent and consequently its phase relations can be represented solely as a function of pressure and temperature. In the second model we eliminate CO_2 from the bulk composition to simulate devolatilization in an open system dominated by an aqueous fluid. In this model, the initial water content determines the onset of dehydration, but once the system becomes water-saturated there is no difference between closed and open system behavior.

Seismic velocity anomalies along the tops of subducted slabs are inferred relative to the velocity in the adjacent mantle. To compute these relative velocities we employ a pyrolitic composition (pyrolite in Table 2, [23]) as a model for the ambient mantle. In order to constrain the P–T con-

Table 2
Model rock compositions in weight proportions normalized relative to 45 parts SiO_2

	Unaltered basalt	Altered basalt	Pyrolite	Lawsonite–eclogite
SiO_2	45.00	45.00	45.00	45.00
TiO_2		1.10	0.71	1.19
Al_2O_3	14.48	15.26	3.52	20.91
FeO	8.16	9.84		10.89
MgO	6.31	6.54	37.33	6.58
CaO	8.65	12.66	3.07	9.57
Na_2O	2.75	2.03	0.57	4.10
K_2O		0.55		0.28
H_2O	saturated	2.63		
CO_2		2.90 or 0.0		

Unaltered basalt is a synthetic high-Mg MORB [15]; altered basalt is an average for the upper 500 m of the igneous section of the oceanic crust [19]; and pyrolite is a model composition originally proposed to represent the mantle beneath Hawaii [23]. The lawsonite–eclogite composition is provided for comparison and is the average of three lawsonite–clinpyroxene–garnet xenoliths that are thought to have derived from subducted metabasic oceanic crust [41].

ditions along the tops of subducted slabs at 100–250 km depth, we extrapolate geotherms estimated for NE and SW Japan [24], which we adopt as limiting low-temperature and high-temperature geotherms, respectively, for circum-Pacific subduction (Fig. 1a) [17,18].

2.1. Computation of seismic velocities

The assemblages, modes and compositions of metamorphic minerals for the model rock compositions were determined by free energy minimization [25,26] using thermodynamic data for pure phases from reference [27] and solution models summarized in Table 3. The compressional- (v_p) and shear-wave (v_s) velocity through an elastically isotropic fluid or homogeneous single crystal are a function of three thermodynamic properties of the phase in question [28,29]:

$$v_P = \sqrt{\frac{K_S + 4\mu/3}{\rho}} \tag{1}$$

$$v_S = \sqrt{\frac{\mu}{\rho}} \tag{2}$$

where ρ is the density, K_S is the adiabatic bulk modulus, and μ is the shear modulus. Conventional thermodynamic databases and solution models are designed for the computation of phase equilibria under isostatic conditions and therefore do not constrain the shear modulus; however, both density and the adiabatic bulk modulus can be expressed as a function of the Gibbs energy for an isostatic system:

$$\rho = N \Big/ \frac{\partial G}{\partial P} \tag{3}$$

$$K_S = -\frac{\partial G}{\partial P}\left[\frac{\partial^2 G}{\partial P^2} + \left(\frac{\partial}{\partial P}\frac{\partial G}{\partial T}\right)^2 \Big/ \frac{\partial^2 G}{\partial T^2}\right]^{-1} \tag{4}$$

where G is the molar free energy and N is the molar formula weight. Thus it is apparent that seismic velocities are dependent on the thermody-

namic function G, which is minimized to establish the amounts and compositions of the phases that are stable as a function of pressure and temperature. Our strategy for the calculation of seismic velocities differs from that of reference [30] in that we evaluate the adiabatic bulk modulus and density from Eqs. 3 and 4 with the thermodynamic data used for computing phase relations. This strategy has the virtue that it maximizes the consistency between the computed phase relations and seismic velocities, and leaves the shear modulus as the only parameter not obtained by the thermodynamic calculations. Shear moduli for stoichiometric phases were computed by the empirical relation:

$$\mu = \mu_0 + T\frac{\partial \mu}{\partial T} + P\frac{\partial \mu}{\partial P} \tag{5}$$

where the parameters μ_0, $\partial\mu/\partial T$, $\partial\mu/\partial P$ are taken to be constants. The shear moduli of solution phases were computed as the arithmetic mean of the moduli of the solution endmembers weighted by the molar proportions of the endmembers. This averaging approach is appropriate for a chemical mixture, whereas the more complex averaging schemes sometimes employed in geophysical computations imply that solution phases are mechanical mixtures.

The programs and data used for the calculation of phase relations and seismic velocities are available at http://www.perplex.ethz.ch. Shear moduli for most phases were taken from reference [9], this database was augmented by shear moduli reported for lawsonite [31], talc [32], stishovite [29], muscovite and carbonates [33]. Where lacking, shear moduli of Fe-endmembers of crystalline solutions were approximated by the moduli of the corresponding Mg-endmember. The P–T dependencies of the shear moduli of muscovite and carbonates were approximated by those of chlorite [9] and calcite [34], respectively, whereas those of lawsonite were taken to be as in reference [9]. Because our concern is with relative seismic velocities, no correction was made for anelasticity [29] and Voight–Reuss–Hill averaging of the velocities of the constituent phases, weighted by volume fraction, was used to compute whole-rock seismic velocities [28].
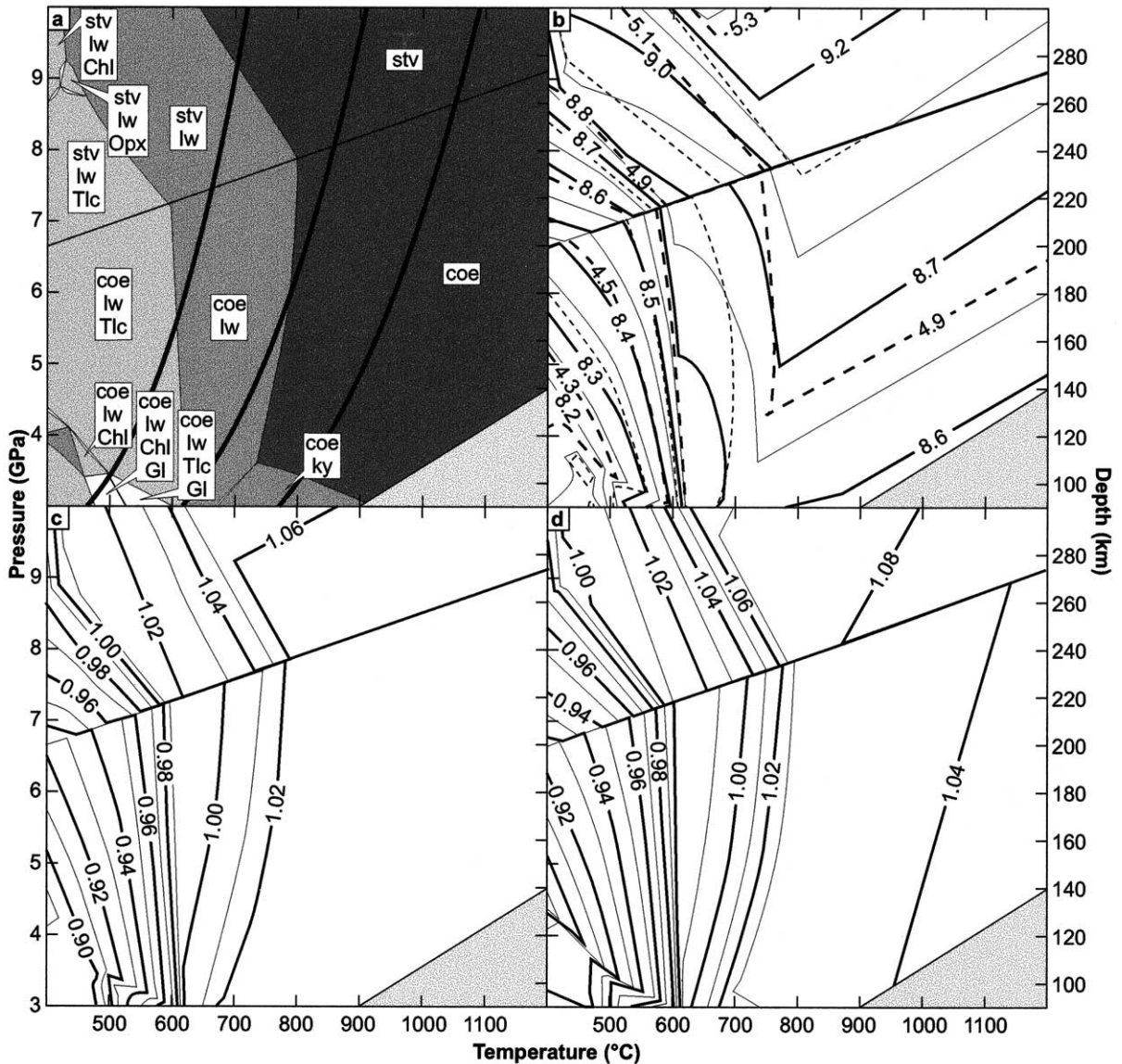
Fig. 1. Computed phase relations and seismic velocities for the unaltered basalt composition (Table 2), assuming water-saturated conditions. See Table 3 for phase notation. The range of seismic velocities computed for six additional MORB compositions [2,16], differs from those depicted by < 1%. a: Phase relations and geothermal gradients; in addition to the phases indicated, clinopyroxene, garnet and water are stable in all fields except the unlabeled phase fields in the lower left corner. The geotherms, discussed in the text, are indicated by thick curves and define the probable range subduction zone conditions. For simplicity the lightly shaded field in the lower right corner masks phase relations involving quartz and sanidine. b: Absolute P-wave (solid) and S-wave (dashed) velocities (km/s). c: Relative P-wave velocity, i.e., v_P/v_P^0 (Table 1). d: Relative S-wave velocity, i.e., v_S/v_S^0.

Assessment of the error associated with our seismic velocity estimates is complicated by the paucity of experimental constraints on the relevant elastic moduli, which are without doubt the dominant source of uncertainty. Where data are available, reported experimental precision leads to a minimum error in computed velocities of 1–2% [33]. However, statistical assessment of the accu-

Table 3
Phase notation, formulae and solution model sources (1 = [45]; 2 = modified from [46]; 3 = [27]; 4 = modified from [47]; 5 = [48])

Symbol	Phase	Formula	Source
arag	aragonite	$CaCO_3$	
Chl	chlorite	$Mg_{(5-y+z)x}Fe_{(5-y+z)(1-x)}Al_{2(1+y-z)}Si_{3-y+z}O_{10}(OH)_8$	1
coe	coesite	SiO_2	
Cpx	clinopyroxene	$Na_yCa_{1-y}Mg_{x(1-y-z)}Fe_{(1-x)(1-y-z)}Al_{y+2z}Si_{2-z}$	2
Dol	dolomite	$CaMg_xFe_{1-x}(CO_3)_2$	3
F	fluid	$(H_2O)_x(CO_2)_{1-x}$	3
Gl	glaucophane	$Ca_{2-2z}Na_zMg_xFe_{(1-x)}Al_{3w+4y}Si_{8-2w-2y}O_{22}(OH)_2$	3
Grt	garnet	$Fe_{3x}Ca_{3y}Mg_{3(1-x-y)}Al_2Si_3O_{12}$	3
H_2O	fluid	H_2O	
ky	kyanite	Al_2SiO_5	
lw	lawsonite	$CaAl_2Si_2O_7(OH)_2 \cdot (H_2O)$	
M	magnesite	$Mg_xFe_{1-x}CO_3$	3
Phg	phengite	$K_xNa_{1-x}Mg_{yw}Fe_{(1-y)w}Al_{3-2w}Si_{3+w}O_{10}(OH)_2$	4
Ol	olivine	$Mg_xFe_{1-x}SiO_4$	3
Opx	orthopyroxene	$Ca_zMg_{x(2-y)(1-z)}Fe_{(1-x)(2-y)(1-z)}Al_{2y}Si_{2-y}O_6$	3
Sa	sanidine	$Na_xK_yAlSi_3O_8$	5
stv	stishovite	SiO_2	
Tlc	talc	$Mg_{(3-y)x}Fe_{(3-y)\,(1-x)}Al_{2y}Si_{4-y}O_{10}(OH)_2$	3

The compositional variables w, x, y, and z may vary between zero and unity and are determined as a function of pressure and temperature by free-energy minimization.

racy of the thermodynamic data used to estimate K_S (T.J.B. Holland, personal communication, 2002) suggests that the standard error on our computed velocities is on the order of 3%. In the case of olivine and orthopyroxene, octahedral Fe–Mg exchange has no systematic effect on bulk moduli but results in a 50% reduction in the shear moduli. Assuming similar effects are present in sheet silicates and clinopyroxene for which the shear moduli are approximated by those of the corresponding Mg-endmembers, the approximation would cause a 2% overestimation of v_S for the Mg-rich compositions relevant here, and the effect would be roughly half as large for v_P. The influence of this effect on the whole-rock velocity would be diminished in proportion to the volume fraction of the mineral. Rock fabric is an additional source of uncertainty: if foliations are developed more strongly within the oceanic crust than in the adjacent mantle, then our model will tend to underestimate the relative seismic velocities within the crust. This inference discounts the possible effects of elastic anisotropy within the constituent minerals.

3. Computational results

Over the range of conditions considered, the computed mineralogy of the pyrolite used as a proxy for the mantle consists of olivine+orthopyroxene+clinopyroxene+garnet+rutile. Computed shear (S-) and compressional (P-) wave velocities for the pyrolite deviate by < 1% from other estimates of mantle seismic velocity [4,28]. These deviations are systematic such that our S-wave and P-wave velocities are lower and higher, respectively, than the earlier estimates. Our velocities are reproduced with a maximum absolute relative error of 0.35% by the expressions:

$$v_P^0 = 8.50 + 6.85 \cdot 10^{-2}P - (5.21 \cdot 10^{-4} - 1.08 \cdot 10^{-5}P)T \tag{6}$$

$$v_S^0 = 4.92 + 3.27 \cdot 10^{-2}P - (3.33 \cdot 10^{-4} - 4.17 \cdot 10^{-6}P)T \tag{7}$$

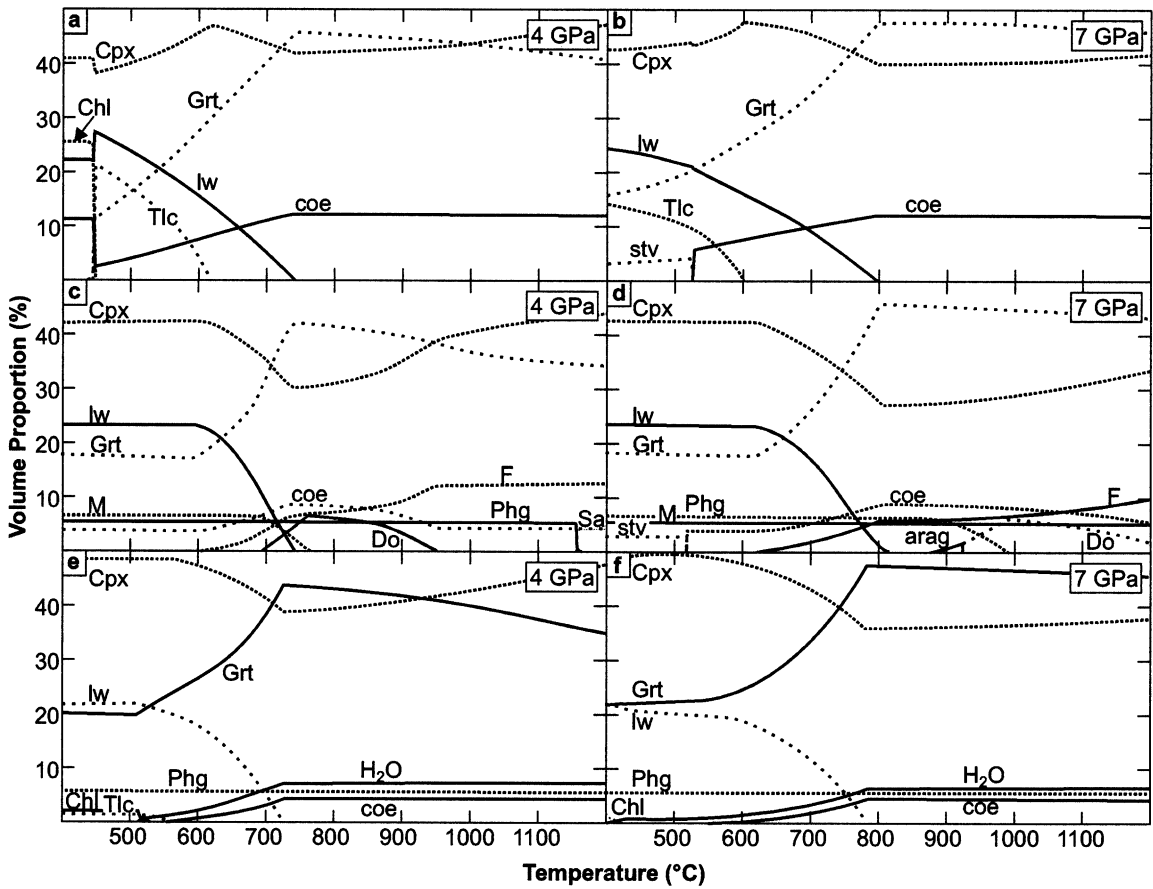where the units for velocity, pressure and temperature are km/s, GPa and K.

Fig. 2. Phase proportions as a function of temperature at 4 and 7 GPa for unaltered metabasalt (a,b), altered carbonate-bearing metabasalt (c,d) and altered CO_2-free metabasalt (e,f) metabasalt. In c–f phase proportions include the fluid phase.

3.1. Unaltered metabasalt

The computed phase equilibria (Fig. 1a) and mineral modes (Fig. 2a, b) for the unaltered metabasalt are in excellent agreement with experimental results on this composition ([15,16], see also [35]), with the exception that talc rather than chloritoid is predicted to be stable at low temperatures. However, the experimental chloritoid occurrence is ambiguous. The relative experimental stability of talc and chloritoid depends on bulk chemistry and there are grounds to suspect that chloritoid was stabilized by disequilibrium Fe–Mg fractionation (S. Poli and M.W. Schmidt, personal communication, 2002). The phase relations for this composition were not investigated at temper-

atures below 650°C. Nonetheless, on the basis of experimental studies [36] on other compositions, it appears probable that the low-temperature, high-pressure computed stability fields of chlorite and orthopyroxene are an artifact of thermodynamic extrapolation.

To assess the sensitivity of our predictions to composition we computed water-saturated phase relations and seismic velocities for six additional MORBs chosen to represent the extremes, primarily through variation of Mg number, for the average composition of the igneous section of the crust [2,16]. Two of the compositions contain potassium, which stabilizes phengite experimentally and in our computations over the conditions spanned by the model geotherms. In the exper-

imental model [16] phengite reacts to produce melts at conditions corresponding approximately to the high-temperature geotherm (Fig. 1a). Because we lack a thermodynamic model for such melts, we are unable to quantify this melting behavior.

For all seven compositions: the predicted thermal limit for lawsonite–eclogites is essentially identical, and differs by < 25°C from the experimental determinations; within the lawsonite stability field talc is stable to 700–720°C, irrespective of pressure; the high-temperature limit of talc stability decays weakly with increasing pressure, intersecting the low-temperature geotherm at pressures of 5–5.5 GPa; and the range of seismic velocity anomalies varies by < 1%. We therefore conclude that our results are robust with respect to compositional variations.

The computed metabasalt seismic velocities demonstrate that metamorphic devolatilization is a first order control on the seismic structure of subducted oceanic crust (Fig. 1b–d), whereby contours of continuous dehydration reaction progress are essentially equivalent to contours of constant velocity. The velocity anomalies (Fig. 1c, d) within the talc+lawsonite field are comparable to those reported for low-velocity layers; however, estimated subduction zone geothermal gradients preclude a role for talc in the origin of low-velocity layers at depths > 160 km. Seismic velocities within lawsonite–eclogites stable at temperatures above the talc stability are similar to those of the ambient mantle.

The coesite–stishovite transition also has a profound effect on seismic velocity of metabasalts. This effect diminishes with falling temperature because the stability of hydrous silica-rich minerals lowers the abundances of the silica polymorphs. In anhydrous basalts the transition induces a 2% increase in the seismic velocity. Thus within the stishovite stability field, basaltic–eclogites have positive velocity anomalies of 4–6%, a range consistent with the Tonga–Kermadec high-velocity layer [2] that extends to a depth of 350 km. Thus, although deep low-velocity layers cannot be explained by typical metabasalt mineralogies, such mineralogies may indeed be the origin of deep high-velocity layers.

3.2. Altered metabasalt

The computed phase relations for the CO_2-bearing altered metabasalt (Figs. 3a and 4a) differ in a number of details from those of the unaltered metabasalt. Most notably, at low temperatures talc is not stable; the phase relations are not fluid-saturated; and although lawsonite stability is restricted to slightly lower temperatures, the abundance of lawsonite is generally greater than for the unaltered basalt. The higher lawsonite abundance reflects the high Ca to Si ratio of the altered basalt (Table 2, [19]). These observations confirm that although bulk composition affects lawsonite abundance in metabasalts, it has only a weak influence on lawsonite stability [16,35].

For the CO_2-bearing metabasalt, devolatilization occurs in two major pulses (Figs. 3a and 2c, d). The low-temperature pulse is dominated by dehydration of lawsonite across the fluid+phengite+magnesite+lawsonite field. The high-temperature pulse is dominated by the decarbonation of dolomite across the fluid+phengite+dolomite field. These devolatilization reactions result in a 4–5% increase in relative P-wave velocity during dehydration and 1–1.5% during decarbonation (Fig. 3c). The larger increase in S-wave velocity during lawsonite decomposition (6–7%, Fig. 3d) is largely due to the high Poisson ratio of lawsonite [31]. These changes are superimposed upon the variation of seismic velocity due to temperature and pressure in the absence of significant devolatilization. At temperatures below the onset of devolatilization, roughly coincident with the low-temperature geotherm, the combined effect of pressure and temperature causes the metabasalt velocities to decrease negligibly with pressure relative to those of the ambient mantle (Fig. 3c, d). Thus the conditions of the low-temperature geotherm define the maximum relative-velocity decrease (4–7%) for the carbonated metabasalt (Fig. 3). Once lawsonite dehydration is complete, the influence of carbonate mineralogy leads to an interval over which seismic velocities rise more rapidly with pressure in metabasalt than in pyrolite. This effect is manifest by a slight (∼1%) positive velocity anomaly for conditions along the intermediate geotherm at pressures beyond
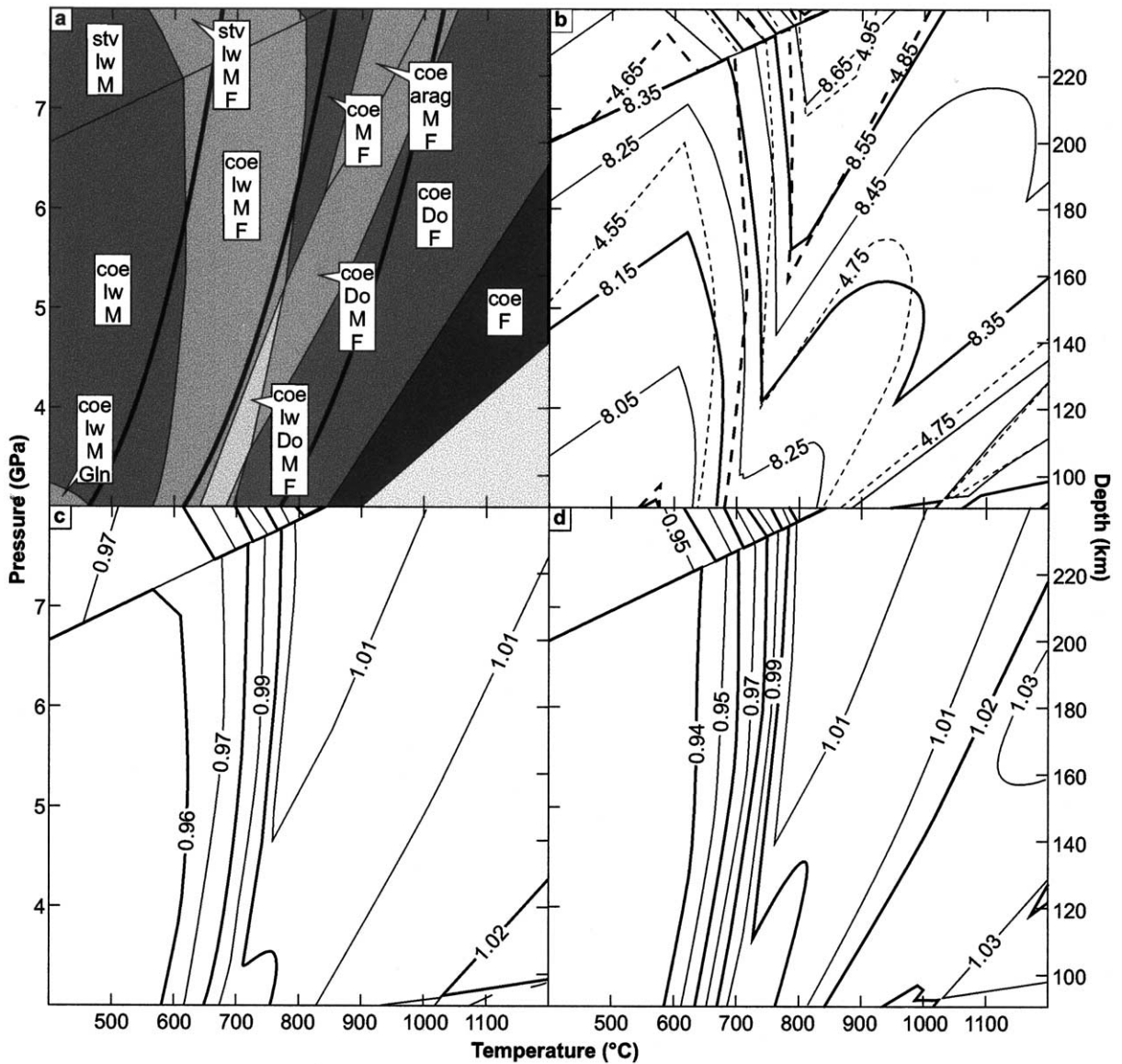
Fig. 3. Computed phase relations and seismic velocities for the carbonate-bearing altered basalt composition (Table 2). Seismic velocities are for the solid aggregate. See Table 3 for phase notation. The closed system model used for the computation results in stability fields for hydrated minerals that differ insignificantly from the maximum stability field possible in an open system; in contrast, carbonate stability fields are significantly smaller than the maximum field possible in an open system. a: Phase relations and geotherms; in addition to the phases indicated, phengite, clinopyroxene, garnet and rutile (< 1 volume %) are present in all fields. The geotherms, discussed in the text, are indicated by thick curves and define the probable range of subduction zone conditions. For simplicity the lightly shaded field in the lower right corner masks phase relations involving quartz and sanidine. b: Absolute P-wave (solid) and S-wave (dashed) velocities (km/s). c: Relative P-wave velocity i.e., v_P/v_P^0 (Table 1). d: Relative S-wave velocity, i.e., v_S/v_S^0.
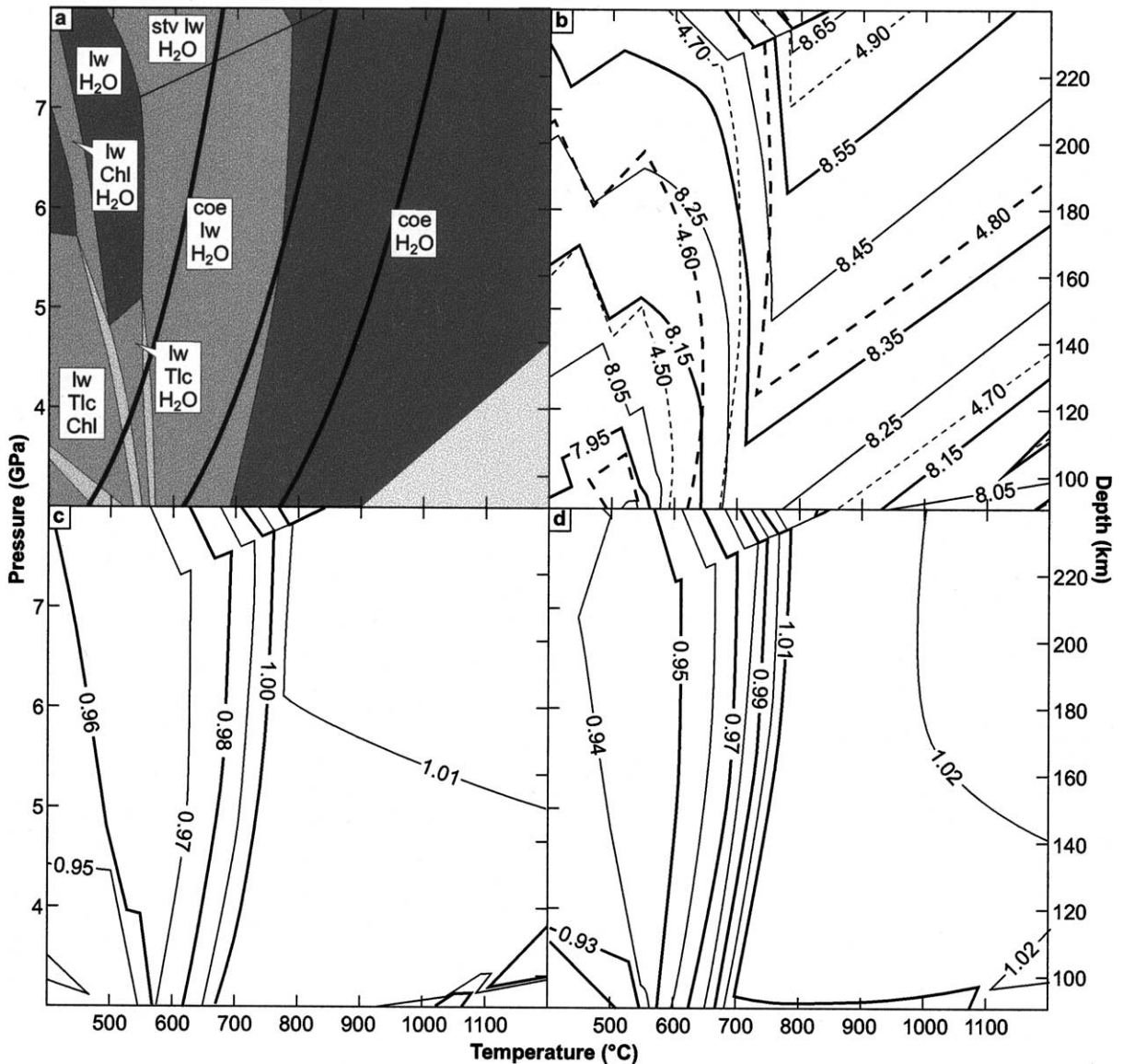
Fig. 4. Computed phase relations and seismic velocities for the CO$_2$-free altered basalt composition (Table 2). Seismic velocities are for the solid aggregate. See Table 3 for phase notation. For fluid-present conditions, the closed system model used here yields identical results to an open system model. a: Phase relations and geotherms; in addition to the phases indicated, phengite, clino-pyroxene, garnet and rutile (<1 volume %) are present in all fields. The geotherms, discussed in the text, are indicated by thick curves and define the probable range subduction zone conditions. For simplicity the lightly shaded field in the lower right corner masks phase relations involving quartz and sanidine. b: Absolute P-wave (solid) and S-wave (dashed) velocities (km/s). c: Rela-tive P-wave velocity, i.e., v_P/v_P^0 (Table 1). d: Relative S-wave velocity, i.e., v_S/v_S^0.

the lawsonite stability field (>6 GPa). The high-temperature geotherm is essentially coincident with conditions for the onset of decarbonation. Discounting the possible influence of fluids, at

these P–T conditions the altered metabasalt would be seismically indistinguishable from ambi-ent mantle. Because decarbonation results in low-ered seismic velocities, a minor negative anomaly

($< 1\%$) is predicted for higher-temperature geotherms.

Phase relations for the CO_2-free altered metabasalt are similar to those of the unaltered basalt, but talc and chlorite modes are minor for the altered metabasalt. The effect of lawsonite dehydration on seismic velocities is comparable to that in the CO_2-bearing altered metabasalt. However, in the CO_2-free model the onset of dehydration occurs at lower temperatures with the result that the low-temperature geotherm does not define the maximum negative velocity anomaly. At conditions along the intermediate geotherm beyond lawsonite stability, and along the entire high-temperature geotherm, there is no significant seismic velocity anomaly. The CO_2-free metabasalt model is water-saturated over almost the entire range of conditions considered. Consequently, the model is an appropriate proxy for an altered metabasalt system that is open with respect to a water-rich fluid.

Both altered metabasalt models predict negative anomalies that decay between the low- and intermediate-temperature geotherms. Carbonate stability introduces some complexity at higher temperatures (Fig. 3b–d), but in the present context the complexity is insignificant. Thus, from a seismic perspective, there is no fundamental difference between the altered metabasalt models and both provide plausible matches with the velocity reductions of 3–7% typically observed beneath the North Pacific Subduction zones. The quality of this match is diminished by the predicted difference in P- and S-wave anomalies due to the properties of lawsonite, whereas no systematic discrepancies in the magnitude of observed P- and S-wave anomalies are observed in seismic studies [8].

4. Discussion

The positive P–T dependence of lawsonite dehydration within the coesite stability field, as opposed to the negative dependence for dehydration of talc, serpentine and chlorite, is a robust feature in all our calculations and is also observed experimentally [16,37,38]. Lawsonite is, thus, unique among hydrous silicates in that its abundance does not vary strongly in response to changing P–T conditions in the range of interest. Consequently, the seismic properties of lawsonite–eclogites may remain constant during subduction, and lawsonite–eclogites are therefore capable of forming a layer with uniform properties at a 100–250 km depth. If the geothermal gradients of Peacock and Wang [24] are valid constraints on subduction zone conditions, then our calculations indicate that other hydrous silicates cannot explain low-velocity layers at depths > 150 km, leaving lawsonite as the sole candidate for a mineralogical origin of low-velocity layers. The apparent depth limit for low-velocity layers in the context of a lawsonite–eclogite model can be attributed to the influence of the coesite–stishovite transition at a depth of 220–240 km. Beyond this transition, the thermal stability of lawsonite decays with increasing pressure, placing an upper limit on the depth range for lawsonite–eclogites ([16], Fig. 1). The continuous dehydration reactions predicted to be stable here do not involve the nucleation of new mineral phases. It is therefore improbable that metastable hydrous phases are an important component of low-velocity layers [13].

Despite the large P–T stability for lawsonite–eclogites predicted here and observed in experimental studies, natural occurrences of lawsonite–eclogites are rare – a fact that is commonly attributed to retrograde consumption of lawsonite during exhumation [39,40]. However, lawsonite–eclogites are preserved as xenoliths in diatreme breccias of the Colorado Plateau [41]. These xenoliths are thought to represent samples of subducted oceanic crust and are identical to the lawsonite+clinpyroxene+garnet mineralogy predicted here for the CO_2-free altered metabasalt (Fig. 4a). The protolith for these xenoliths, which contain up to 50 volume % lawsonite, is a metabasic rock that is somewhat more intensely altered (Table 2) than our altered basalt composition but yields similar seismic velocities. The existence of these xenoliths provides reassurance not only that lawsonite–eclogites exist in natural subduction zone settings, but also that intense alteration is not atypical of such rocks.

We have explored the influence of metamor-

phism on the seismic structure of the oceanic crust for altered and unaltered basaltic compositions. The seismic velocities computed for unaltered compositions cannot explain low-velocity layers at depths > 100 km; but at depths beyond the coesite–stishovite transition, the predicted anomalously high velocities match the properties of the Tonga–Kermadec high-velocity layer [2]. In contrast, the seismic velocities for lawsonite–eclogites derived from hydrothermally altered metabasalts do provide a reasonable match for circum-Pacific low-velocity layers. This result is relatively insensitive to uncertainties regarding carbonate stability, because seismic velocities in carbonate minerals are similar to those of the ambient mantle.

Our models support the contention that low-velocity layers represent the subduction of substantial amounts of volatiles beyond sub-arc depths [7,8], but we find no necessity for appealing to disequilibrium to explain this phenomenon. A weak link in the association of low-velocity layers with hydrous minerals is that the most probable candidates, lawsonite, talc and serpentine, are all characterized by high values of Poisson's ratio [31,8,32]. Consequently, the S-wave velocity anomalies should be 1–2% larger than the corresponding P-wave anomaly, but such systematic differences are not observed [8]. Given that strong foliations may develop in natural lawsonite–eclogites [39,41], the extraordinary elastic anisotropy of lawsonite [31] may explain the absence of such discrepancies if lawsonite–eclogites are indeed the cause of low-velocity layers. In this regard, it is pertinent to recall that our model for the ambient mantle yields up to 1% lower S-wave and 1% higher P-wave velocities than the estimates used by reference [8]. Thus, the discrepancy in the magnitudes of the P- and S-wave anomalies may simply be illusory.

The association of hydrous minerals with deep low-velocity layers limits subduction zone temperatures toward the lower bounds estimated for circum-Pacific subduction [24]. In view of the stringency of this constraint the potential influence of fluids must be admitted as an alternative hypothesis for the origin of the low-velocity layers [7,42]. Metabasalt devolatilization may generate 10–20 volume % fluid (Fig. 2c–f) that is a potential cause

of intermediate-depth earthquakes [11]. The foci and mechanisms of such earthquakes locate low-velocity layers within the subducted slab [6,7,43], supporting correlation of low-velocity layers with subducted metabasalts. These observations mitigate against models in which low-velocity layers are caused by hydration of the mantle above the subducted oceanic slab [32,44]. Because the fate of the fluids released by devolatilization is a subject of conjecture, we make no attempt to evaluate its influence on seismic velocities other than to remark that fluid retention within the rock matrix would cause more negative velocity anomalies than those predicted here for the solid residuum [8,42]. The evaluation of these effects awaits a more detailed understanding of the processes by which fluids are expelled from subduction zones.

Acknowledgements

References

[1] Y. Fukao, K. Kanjo, I. Nakamura, Deep seismic zone as an upper mantle reflector of body waves, Nature 272 (1978) 606–608.

[2] D. Gubbins, A. Barnicoat, J. Cann, Seismological constraints on the gabbro-eclogite transition in subducted oceanic crust, Earth Planet. Sci. Lett. 122 (1994) 89–101.

[3] T. Matsuzawa, A. Umino, A. Hasegawa, A. Takagi, Estimation of the thickness of the low velocity layer at the surface of the descending oceanic plate beneath the Northeastern Japan arc by using synthesized PS-wave, Tohoku Geophys. J. 31 (1987) 19–28.

[4] G. Helffrich, S. Stein, Study of the structure of the slab-mantle interface using reflected and converted seismic waves, Geophys. J. Int. 115 (1993) 14–40.

[5] G.A. Abers, G. Sarker, Dispersion of regional body waves at 100–150 km depth beneath Alaska: in situ constraints on metamorphism in the subducted crust, Geophys. Res. Lett. 23 (1996) 1171–1174.

[6] G. Helffrich, G.A. Abers, Slab low-velocity layer in the eastern Aleutian subduction zone, Geophys. J. Int. 130 (1997) 640–648.

[7] C.H. Lin, B.S. Huang, R.J. Rau, Seismological evidence for a low-velocity layer within the subducted slab of southern Taiwan, Earth Planet. Sci. Lett. 174 (1999) 231–240.

[8] G.A. Abers, Hydrated subducted crust at 100–250 km depth, Earth Planet. Sci. Lett. 176 (2000) 323–330.

[9] G. Helffrich, Suducted lithospheric slab velocity structure: observations and mineralogical inferences, in: G.E. Bebout, D.W. Scholl, S.H. Kirby, J.P. Platt (Eds.), Subduction Top to Bottom, Geophys. Monogr. 96, American Geophysical Union, 1996, pp. 215–222.

[10] S. Hori, H. Inoue, Y. Fukao, M. Ukawa, Seismic detection of the untransformed 'basaltic' oceanic crust subducting into the mantle, Geophys. J. Royal Astron. Soc. 83 (1985) 169–197.

[11] S.H. Kirby, E.R. Engdahl, R. Denlinger, Intraslab earthquakes and arc volcanism: dual expressions of crustal and uppermost mantle metamorphism in subducting slabs., in: G.E. Bebout, D.W. Scholl, S.H. Kirby, J.P. Platt (Eds.), Subduction Top to Bottom, Geophys. Monogr. 96, Am. Geophys. Union, Washington DC, 1996, pp. 195–214.

[12] D.C. Rubie, A.B. Thompson, Kinetics of metamorphic reactions, in: A.B. Thompson and D.C. Rubie (Eds.), Metamorphic Reactions: Kinetics, Textures, and Deformation, Springer, New York, 1985, pp. 291.

[13] D.C. Rubie, Disequilibrium during metamorphism: the role of nucleation kinetics, in: P.J. Treolar, P.J. O'Brien (Eds.), What Drives Metamorphism and Metamorphic Reactions?, Geol. Soc., London, 1998, pp. 199–214.

[14] J.C. Alt, Subseafloor processes in mid-ocean ridge hydrothermal systems, in: S.E. Humphris, R.A. Zierenberg, L.S. Millineaux, R.E. Thompson (Eds.), Seafloor Hydrothermal Systems: Physical, Chemical, Biological and Geological Interactions, Geophys. Monogr. 91, Am. Geophys. Soc., 1995, pp. 85–114.

[15] S. Poli, M.W. Schmidt, H_2O transport and release in subduction zones: experimental constraints on basaltic and andesitic systems, J. Geophys. Res. 100 (1995) 22299–22314.

[16] M.W. Schmidt, S. Poli, Experimentally based water budgets for dehydrating slabs and consequences for arc magma generation, Earth Planet. Sci. Lett. 163 (1998) 361–379.

[17] D.M. Kerrick, J.A.D. Connolly, Metamorphic devolatilization of subducted marine sediments and transport of volatiles to the Earth's mantle, Nature 411 (2001) 293–296.

[18] D.M. Kerrick, J.A.D. Connolly, Metamorphic devolatilization of subducted oceanic metabasalts implications for seismicity, arc magamatism and volatile recycling, Earth Planet. Sci. Lett. 189 (2001) 19–29.

[19] H. Staudigel, S. Hart, H. Schmincke, B. Smith, Cretaceous ocean crust at DSDP sites 417–418: carbon uptake from weathering versus loss by magmatic outgassing, Geochim. Cosmochim. Acta 53 (1989) 3091–3094.

[20] J.C. Alt, D.A.H. Teagle, The uptake of carbon during alteration of oceanic crust, Geochim. Cosmochim. Acta 63 (1999) 1527–1535.

[21] T. Matsuzawa, Intermediate depth earthquakes and upper mantle structure beneath the Northeastern Japan arc, Trans. Am. Geophys. Union 71 (1990) 947.

[22] R.L. Carlson, Lower crustal water contents, P-wave velocities, and modal mineralogy of oceanic diabase and gabbro, Trans. Am. Geophys. Union 82 (2001) 1154.

[23] I. Jackson, S.M. Rigden. Composition and temperature of the Earth's mantle: seismological models interpreted through experimental studies of Earth materials, in: I. Jackson (Ed.), The Earth's Mantle: Composition, Structure and Evolution, Cambridge University Press, Cambridge, 1998.

[24] S.M. Peacock, K. Wang, Seismic consequences of warm versus cool subduction metamorphism: examples from southwest and northeast Japan, Science 286 (1999) 937–939.

[25] J.A.D. Connolly, Multivariable phase diagrams an algorithm based on generalized thermodynamics, Am. J. Sci. 290 (1990) 666–718.

[26] J.A.D. Connolly, K. Petrini, An automated strategy for calculation of phase diagram sections and retrieval of rock properties as a function of physical conditions, J. Metamorph. Geol. 20 (2002) 697–708.

[27] T.J.B.H. Holland, R. Powell, An internally consistent thermodynamic data set for phases of petrological interest, J. Metamorph. Geol. 16 (1998) 309–343.

[28] C.R. Bina, G. Helffrich, Calculation of elastic properties from thermodynamic equation of state principles, Annu. Rev. Earth Planet. Sci. 20 (1992) 527–552.

[29] B.B. Karki, L. Sixtrude, R.M. Wentzcovitch, High pressure elastic properties of major materials of Earth's mantle from first principles, Rev. Geophys. 39 (2001) 507–534.

[30] S.V. Sobolev, A.Y. Babeyko, Modeling of mineralogical composition, density, and elastic-wace velocities in anhydrous magmatic rocks, Surv. Geophys. 15 (1994) 515–544.

[31] S.V. Sinogeikin, F.R. Schilling, J.D. Bass, Single crystal elasticity of lawsonite, Am. Mineral. 85 (2000) 1834–1837.

[32] E. Bailey, J.R. Holloway, Experimental determination of elastic properties of talc to 800 degrees C, 0.5 GPa: calculations of the effect on hydrated peridotite, and implications for cold subduction zones, Earth Planet. Sci. Lett. 183 (2000) 487–498.

[33] J.D. Bass, Elasticity of minerals, melts and glasses, in: T.J. Ahrens (Ed.), Mineral Physics and Crystallography: A Handbook of Physical Constants, Reference Shelf 2, Am. Geophys. Union, 1995, pp. 45–63.

[34] R.F.S. Hearmon, The elastic constants of crystals and other anisotropic materials, in: K.H. Hellwege, A.M.

Hellwege (Eds.), Landolt–Börnstein Tables, III, 11, 1979, pp. 1–244.

[35] K. Okamoto, M. Shigenori, The high pressure synthesis of lawsonite in the MORB+H2O system, Am. Mineral. 84 (1999) 363–373.

[36] G.D. Bromiley, A. Pawley, The high-pressure stability of Mg-surassite in a model hydrous peridotite: a possible mechanism for the deep subduction of significant volumes of H_2O, Contrib. Mineral. Petrol. 142 (2002) 714–723.

[37] K. Bose, J. Ganguly, Experimental and theoretical studies of the stabilities of talc, antigorite and phase A at high pressures with applications to subduction processes, Earth Planet. Sci. Lett. 136 (1995) 109–121.

[38] P. Ulmer, V. Trommsdorff, Serpentine stability to mantle depths and subduction-related magmatism, Science 268 (1995) 858–861.

[39] E.D. Ghent, M.Z. Stout, P. Erdmer, Pressure-temperature evolution of lawsonite-bearing eclogites, Pinchi Lake, British Columbia, J. Metamorph. Geol. 11 (1993) 279–290.

[40] M.W. Schmidt, S. Poli, The stability of lawsonite and zoisite at high pressures: experiments in CASH to 92 kbar and implications for the presence of hydrous phases in subducted lithosphere, Earth Planet. Sci. Lett. 124 (1994) 105–118.

[41] H. Helmstaedt, D.J. Schulze, Eclogite-facies ultramafic xenoliths from Colorado Plateau diatreme breccias: comparison with eclogits in crustal environments, evaluation of the subduction zone hypothesis, and implications for eclogite xenoliths from diamondiferous kimberlites, in:

D.C. Smith (Ed.), Eclogites and Eclogite–Facies Rocks: Developments in Petrology 12, Elsevier, Amsterdam, 1988, pp. 387–450.

[42] G.R. Helffrich, S. Stein, B.J. Wood, Subduction zone thermal structure and mineralogy and their relationship to seismic-wave reflections and conversions at the slab mantle interface, J. Geophys. Res. 94 (B1) (1989) 753–763.

[43] D.P. Zhao, A. Hasegawa, S. Horiuchi, Tomographic imaging of P and S wave velocity structure beneath north-eastern Japan, J. Geophys. Res. 97 (1992) 19909–19928.

[44] Y. Tatsumi, K. Iti, A. Goto, Elastic wave velocities in an isochemical granulite and amphibolite: origin of a low-velocity layer at the slab/mantle interface, Geophys. Res. Lett. 21 (1994) 17–20.

[45] T. Holland, J. Baker, R. Powell, Mixing properties and activity-composition relationships of chlorites in the system MgO-FeO-Al_2O_3-SiO_2-H_2O, Eur. J. Mineral. 10 (1998) 395–406.

[46] T. Gasparik, Experimental study of subsolidus phase relations and mixing properties of pyroxene and plagioclase in the system Na_2O-CaO-Al_2O_3-SiO_2, Contrib. Mineral. Petrol. 89 (1985) 346–357.

[47] N.D. Chatterjee, E. Froese, A thermodynamic study of the pseudo-binary join muscovite-paragonite in the system $KAlSi_3O_8$-$NaAlSi_3O_8$-Al_2O_3-SiO_2-H_2O, Am. Mineral. 60 (1975) 985–993.

[48] J.B. Thompson, D.R. Waldbaum, Mixing properties of sanidine crystalline solutions. IV. Phase diagrams from equations of state, Am. Mineral. 76 (1969) 493–500.